J Mol Model (2013) 19:3095–3102
DOI 10.1007/s00894-013-1838-4

ORIGINAL PAPER

Electron correlation effects and density analysis of the first-order hyperpolarizability of neutral guanine tautomers

Andrea Alparone

Received: 29 January 2013 / Accepted: 21 March 2013 / Published online: 20 April 2013

Abstract Dipole moments (μ), charge distributions, and static electronic first-order hyperpolarizabilities (β_μ) of the two lowest-energy keto tautomers of guanine (**7H** and **9H**) were determined in the gas phase using Hartree–Fock, Møller–Plesset perturbation theory (MP2 and MP4), and DFT (PBE1PBE, B97-1, B3LYP, CAM-B3LYP) methods with Dunning's correlation-consistent aug-cc-pVDZ and *d*-aug-cc-pVDZ basis sets. The most stable isomer **7H** exhibits a μ value smaller than that of the **9H** form by a factor of ca. 3.5. The β_μ value of the **9H** tautomer is strongly dependent on the computational method employed, as it dramatically influences the β_μ (**9H**)/β_μ (**7H**) ratio, which at the highest correlated MP4/aug-cc-pVDZ level is predicted to be ca. 5. The Coulomb-attenuating hybrid exchange-correlation CAM-B3LYP method is superior to the conventional PBE1PBE, B3LYP, and B97-1 functionals in predicting the β_μ values. Differences between the largest diagonal hyperpolarizability components were clarified through hyperpolarizability density analyses. Dipole moment and first-order hyperpolarizability are molecular properties that are potentially useful for distinguishing the **7H** from the **9H** tautomer.

Keywords Guanine tautomers · Dipole moments · Hyperpolarizability · Density analysis · Møller–Plesset calculations · DFT calculations

Electronic supplementary material The online version of this article (doi:10.1007/s00894-013-1838-4) contains supplementary material, which is available to authorized users.

A. Alparone (✉)
Department of Chemistry, University of Catania,
viale A. Doria 6, Catania 95125, Italy
e-mail: agalparone@unict.it

Introduction

Guanine is a fundamental purine base that is found in the nucleic acids of living organisms and hypothesized to be a preferred target site for mutagens and carcinogens [1, 2]. There are some indications that spontaneous genetic mutations could be controlled by disfavored or rare tautomers constituting DNA base pairs [3–5]. Under physiological conditions, guanine predominantly exists in gas and aqueous phases as neutral keto conformations [6–19]. However, along with these ketonic tautomers, other guanine structures—specifically enolic and imino-oxo forms—have been identified experimentally through spectroscopic techniques [7–9, 20–29].

DNA-based materials have attracted great attention for photonic and nanoelectronic applications [30–39], and have shown interesting nonlinear optical (NLO) properties [38, 39]. In particular, a guanine-based system such as G_4-DNA, which has a guanine-quadruplex structure, is considered an excellent conductor that is potentially suitable for fabricating biomolecular nanowires due to its remarkable polarizability and mechanical rigidity [37].

Characterizations of the electric response properties of guanine have so far been limited to some experimental and theoretical estimates of the electronic polarizability (α) [40–47] and second-order hyperpolarizability (γ) [47]. According to recent MP4/aug-cc-pVDZ calculations [47], the average α and γ values for the lowest-energy guanine tautomers are rather close to each other: within 0.4 % and 5.6 %, respectively. Thus, these physicochemical properties are unable to unambiguously distinguish between guanine tautomers. On the other hand, there are many indications in literature that electronic first-order hyperpolarizabilities (β) and NLO second-

harmonic generation (SHG) properties are strongly dependent on molecular conformation, which implies that they are potentially useful for discriminating between structurally different isomers [48–58]. To the best of our knowledge, electronic β values of guanine tautomers are unknown, whereas Seal et al. [59] recently conducted a computational investigation of the electronic β values of the cytosine–guanine pair.

In the work described in the present paper, we determined the dipole moments (μ), atomic charge distributions, and electronic β values of the most stable keto tautomers of guanine in the gas phase (Fig. 1), investigating the effects of their structures on their electrical properties. Electronic hyperpolarizabilities are usually calculated through ab initio and density functional theory (DFT) methods. However, it is well recognized that conventional DFT methods present severe shortcomings when they are employed to predict electronic hyperpolarizabilities, particularly for π-conjugated compounds [60]. This incorrect behavior originates from the so-called self-interaction error in the exchange term, as it fails to appropriately predict response electric properties which involve nonlocal effects. In general, conventional DFT methods systematically overestimate electronic hyperpolarizabilities, especially for extended π-conjugated chains. To partially circumvent this deficiency, hyperpolarizability computations can be performed using long-range corrected functionals that incorporate certain contributions of the exact Hartree–Fock (HF) exchange potential in the long-range interaction component [61].

The theoretical methods employed in this work are HF, Møller–Plesset perturbation theory (MPn, n=2 and 4), and various levels of DFT. Besides the conventional B3LYP [62, 63], PBE1PBE [64], and B97-1 [65] functionals, we used the Coloumb-attenuating hybrid exchange-correlation CAM-B3LYP method [66]. The CAM-B3LYP functional has been employed with success to predict electronic (hyper)polarizabilities [47, 67–74], and its application leads to substantially improved performance over the traditional DFT methods when reproducing high-level ab initio computations. The performances of the DFT functionals were evaluated in the present work with respect to the ab initio correlated MP4 level.

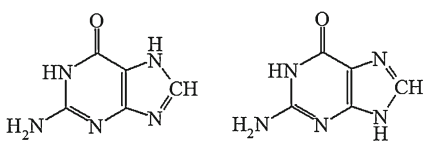

Fig. 1 Molecular structures of guanine tautomers

Computational details

All calculations were carried out with the Gaussian 09 [75] and GAMESS programs [76]. The structures were optimized in the vacuum using the B97-1 functional with the aug-cc-pVDZ basis set [77]. The B97-1 method was previously used with success to determine the geometries of heterocycles [78–80]. Cartesian coordinates of the **7H** and **9H** tautomers are given in the "Electronic supplementary material" (ESM; Tables S1 and S2), whereas a selection of the calculated geometrical parameters are reported in Fig. 2, together with the available experimental data [81]. The agreement between the B97-1/aug-cc-pVDZ and experimental geometries is reasonable, considering that the present structures refer to isolated molecules while the observed data were determined via X-ray measurements [81]. Vibrational analysis confirmed that both of the investigated tautomers are true minima on the potential energy surfaces (no imaginary wavenumbers). Static electronic β values were obtained analytically at the HF level by means of the time-dependent HF (TD-HF) method [82]. Correlated ab initio (MP2 and MP4) and DFT (B3LYP, B97-1, PBE1PBE and CAM-B3LYP) β values were computed numerically using the finite-field (FF) differentiation approach illustrated by Kurtz et al. [83], using an electric field strength (F) of 0.005 a.u. In order to check the accuracy of the numerical procedure, we compared the β values calculated at the HF level by the TD-HF and FF-HF approaches. All calculations were performed using the polarized and diffuse aug-cc-pVDZ and doubly augmented d-aug-cc-pVDZ Dunning's correlation-consistent basis sets [77, 84]. These basis sets have proven to be adequate for response electric property calculations [41, 47, 72, 79, 80, 85–89].

In this work, we determined dipole moments and first-order hyperpolarizabilities aligned along the direction of the molecular dipole moment (β_μ), which were defined as follows:

$$\mu = \sqrt{\mu_x^2 + \mu_y^2 + \mu_z^2} \tag{1}$$

$$\beta_\mu = \sum_{i=x,y,z} \beta_i \mu_i / |\mu| \tag{2}$$

where β_i (i=x, y, z) is given by $\beta_i = \frac{1}{3} \sum_{j=x,y,z} \left(\beta_{ijj} + \beta_{jij} + \beta_{jji}\right)$.

Atomic units are used throughout the work. Conversion factors to SI units are: 1 a.u. of F ($E_h e^{-1} a_0^{-1}$)=5.142208×10^{11} Vm^{-1}; 1 a.u. of μ (ea_0)=8.478358×10^{-30} Cm; 1 a.u. of β ($e^3 a_0^3 E_h^{-2}$)=3.206361×10^{-53} C^{3}m^{3}J^{-2}.

Results and discussion

As widely documented in the literature [6–19, 47], the **7H** ketonic structure (Fig. 1) is the lowest-energy tautomer of

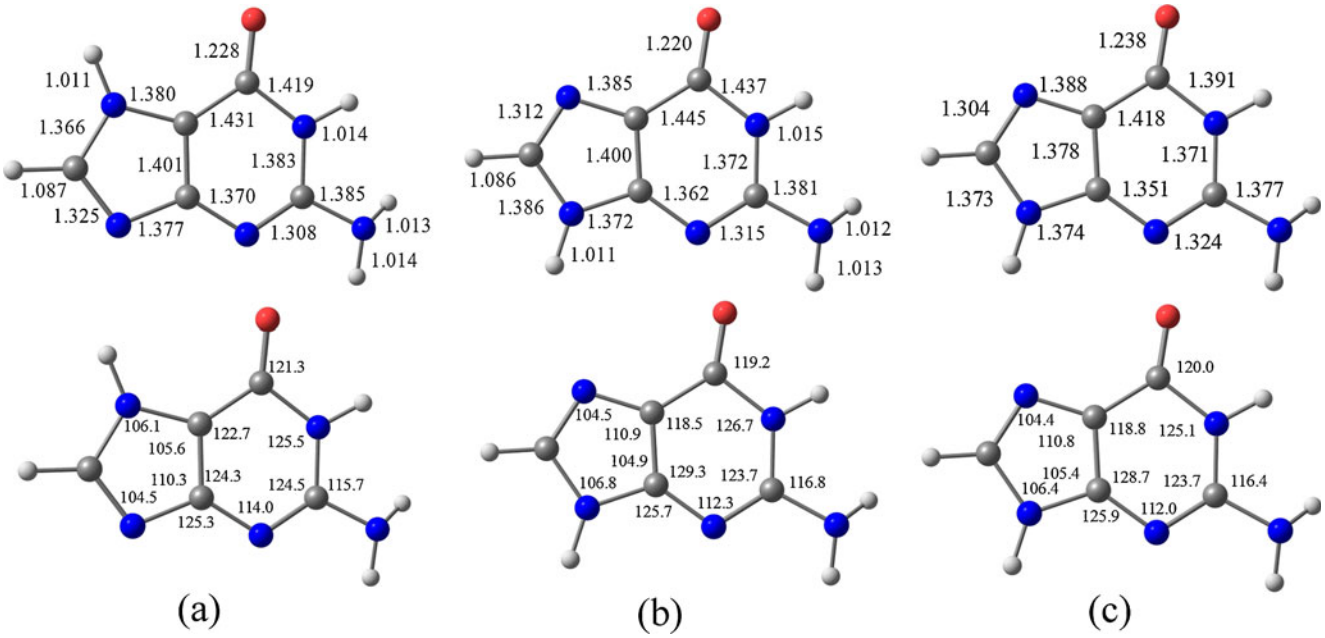

Fig. 2a–c Selected bond lengths (Å, *top*) and bond angles (°, *bottom*) of the guanine tautomers. **a** Gas-phase B97-1/aug-cc-pVDZ data for the **7H** tautomer. **b** Gas-phase B97-1/aug-cc-pVDZ data for the **9H** tautomer. **c** X-ray diffraction data taken from [81]. Color code: *white* hydrogen, *gray* carbon, *red* oxygen, *blue* nitrogen (color figure provided online)

guanine in the gas phase. At the B97-1/aug-cc-pVDZ level, the **9H** tautomer is predicted to lie 0.73 kcal/mol^{-1} above the **7H** structure (0.61 kcal/mol^{-1} when considering the relative free energy values at T=298 K), in excellent agreement with CCSD(T)/aug-cc-pVDZ//RI-MP2/TZVPP calculations (relative energy of 0.69 kcal/mol^{-1}) [6]. Tables 1 and 2 list the μ and β values of the **7H** and **9H** forms. We investigated basis set effects at the HF level for the **9H** isomer. When enlarging the aug-cc-pVDZ to the *d*-aug-cc-pVDZ basis set, one observes only marginal effects on the calculated properties. In fact, the μ values with the two basis sets are identical (2.78 a.u.), whereas β_μ varies by 6 %. Note that the present hyperpolarizability calculations performed using the *d*-aug-cc-pVDZ basis set require approximately four times as much CPU

Table 1 Dipole moments (μ) and static electronic first-order hyperpolarizabilities (β) of the **7H** tautomer of guanine

	HF	MP2	MP4	B3LYP	B97-1	PBE1PBE	CAM-B3LYP
μ_x	0.47	0.46	0.45	0.50	0.51	0.51	0.50
μ_y	−0.23	−0.49	−0.43	−0.32	−0.32	−0.33	−0.35
μ_z	−0.35	−0.34	−0.34	−0.33	−0.33	−0.33	−0.34
μ	0.63	0.75	0.71	0.68	0.69	0.69	0.70
β_{xxx}	93.4	162.0	154.6	85.2	87.6	92.6	114.9
β_{xyy}	−22.8	−6.4	−16.6	−13.9	−13.5	−13.4	−12.7
β_{xzz}	8.5	−1.8	−6.2	−10.8	−10.4	−9.7	−7.8
β_{yxx}	89.2	108.5	129.6	87.0	86.8	86.9	99.3
β_{yyy}	−94.3	1.0	−20.0	−58.1	−58.8	−55.4	−55.2
β_{yzz}	−22.6	−28.5	−26.1	−31.2	−30.5	−28.9	−28.1
β_{xxz}	4.9	7.3	7.3	13.8	12.4	11.0	6.5
β_{yyz}	2.4	3.5	3.1	4.0	3.9	3.7	2.9
β_{zzz}	−1.1	0.9	0.5	1.5	1.3	1.0	−0.5
β_x	79.1	153.8	131.8	60.6	63.7	69.6	94.4
β_y	−27.7	81.0	83.5	−2.4	−2.5	2.7	15.9
β_z	6.2	11.7	10.9	19.3	17.6	15.8	9.0
β_μ	65.8	36.1	27.7	36.3	39.8	42.6	55.1

Calculations were carried out on the B97-1/aug-cc-pVDZ geometry. Basis set: aug-cc-pVDZ. All values are expressed in a.u.

Table 2 Dipole moments (μ) and static electronic first-order hyperpolarizabilities (β) of the **9H** tautomer of guanine

	HF	MP2	MP4	B3LYP	B97-1	PBE1PBE	CAM-B3LYP
μ_x	1.30 (1.29)	1.15	1.19	1.23	1.24	1.24	1.25
μ_y	2.44 (2.44)	2.17	2.19	2.28	2.27	2.28	2.30
μ_z	−0.33 (−0.33)	−0.31	−0.31	−0.30	−0.30	−0.30	−0.31
μ	2.78 (2.78)	2.48	2.51	2.61	2.60	2.61	2.64
β_{xxx}	124.6 (120.5)	200.9	207.8	100.9	103.6	110.5	144.5
β_{xyy}	−53.4 (−53.5)	−27.9	−43.1	−42.0	−41.4	−40.8	−39.5
β_{xzz}	21.4 (20.5)	3.9	1.2	0.1	−0.4	−0.3	2.4
β_{yxx}	41.2 (41.4)	100.2	103.4	38.9	41.5	44.1	63.9
β_{yyy}	−56.9 (−57.4)	−7.4	−18.9	−72.4	−70.8	−63.4	−40.6
β_{yzz}	−17.3 (−14.7)	−25.1	−22.1	−27.2	−26.3	−24.9	−22.4
β_{xxz}	5.4 (5.5)	8.3	7.9	15.7	14.0	12.4	7.3
β_{yyz}	2.9 (2.7)	3.7	3.6	4.5	4.5	4.2	3.4
β_{zzz}	−0.9 (−0.8)	1.4	0.8	1.7	1.5	1.1	−0.2
β_x	92.6 (87.5)	177.8	165.9	59.0	61.9	69.4	107.4
β_y	−33.0 (−30.7)	67.8	62.4	−60.7	−55.6	−44.2	0.9
β_z	7.4 (7.3)	13.4	12.2	21.8	20.1	17.6	10.5
β_μ	13.5 (12.8)	140.1	131.6	−27.7	−21.3	−7.8	50.4

Calculations were carried out on the B97-1/aug-cc-pVDZ geometry. Basis set: aug-cc-pVDZ. Values in parentheses refer to the HF/*d*-aug-cc-pVDZ calculations. All values are expressed in a.u.

time as those performed using the aug-cc-pVDZ basis set. Thus, the aug-cc-pVDZ basis set can be considered a good compromise between accuracy and computational cost, and was used for all subsequent ab initio and DFT calculations.

Dipole moments and charge distributions

At the MP4/aug-cc-pVDZ (MP2/aug-cc-pVDZ) level, the μ values are predicted to be 0.71 a.u. (0.75 a.u.) and 2.51 a.u. (2.48 a.u.) for the **7H** and **9H** tautomers, respectively. The calculated μ data for the **9H** form are overestimated, considering the experimental value of 2.17 a.u. previously obtained in dioxane solution [90]. On the other hand, our μ values are in excellent agreement with previous theoretical estimates computed in the gas phase: 0.79 and 2.48 a.u. at the MP2/6-311++G(d,p)//B3LYP/6-311++G(d,p) level [8] and 0.70 and 2.48 a.u. at the MP2/aug-cc-pVDZ//MP2/aug-cc-pVDZ level [12] for the **7H** and **9H** tautomers, respectively. The effects of electron correlation, which were evaluated by comparing HF vs. MP4, are modest (ca. 10 %). The DFT methods gave similar values of μ (to within 1 %), and adequately reproduced the MP4 figures (to within 5 %).

As can be appreciated by reviewing the data in Tables 1 and 2, both the magnitude and direction of the μ vector are noticeably influenced by the molecular conformation. In fact, when going from the **7H** to **9H** tautomer, the μ value increases by a factor of approximately 3.5. To qualitatively interpret the dominant bond moment contributions to μ, we performed a natural population analysis (NPA) [91]. The NPA atomic charges were computed at the MP2/aug-cc-pVDZ level and the results are given in Fig. 3. The figure also displays the vectorial representation of μ (green arrow). For the **7H** tautomer, the bond moment of the N_7–H bond of the imidazole ring is roughly parallel with although in mutual opposition to other polar bonds: the C=O and N–H bonds of the amino group (see the red arrows in Fig. 3). As a consequence, the dipolar contributions tend to cancel each other out, resulting in a relatively modest μ value (ca. 0.7 a.u.). By contrast, the μ

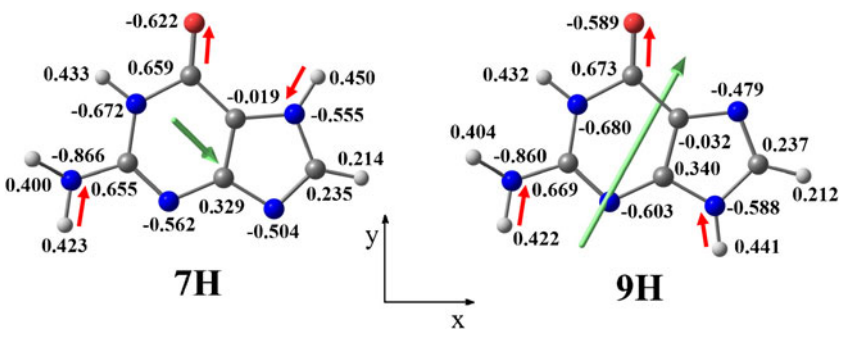

Fig. 3 Dipole moments (*green arrows*) and NPA atomic charges (*e*) of the guanine tautomers. MP2/aug-cc-pVDZ results. Color code: *white* hydrogen, *gray* carbon, *red* oxygen, *blue* nitrogen (color figure provided online)

value of the **9H** tautomer is predicted to be substantially greater: ca. 2.5 a.u. For this structure, the above polar groups constructively contribute to the dominant μ_y component, which represents ca. 90 % of the total μ value. Thus, in polar media, the relative stabilities of the investigated tautomers are expected to change. Indeed, calculations in aqueous solution indicate that the **9H** tautomer is more stable than the **7H** form [6, 10, 13, 14, 16, 47].

Electronic first-order hyperpolarizabilities

In contrast to the μ data, the first-order hyperpolarizabilities are much more affected by the computational method. The evolution of the calculated β_μ values as a function of the theoretical level is illustrated in Fig. 4. At the HF/aug-cc-pVDZ level, β_μ(**7H**)>β_μ(**9H**) and the β_μ(**9H**)/β_μ(**7H**) ratio is predicted to be ca. 0.2. The electron correlation effects (evaluated by comparing the HF and MP4 data) are conspicuous, although they are not uniform for the investigated isomers. However, it is important to note that the HF and MP4 β_μ values are positive for both guanine forms. For the **9H** tautomer, the β_μ value enhances by an order of magnitude upon shifting from the HF/aug-cc-pVDZ to the MP4/aug-cc-pVDZ level, whereas the correlated β_μ value for **7H** decreases by approximately a factor of two. As a result, at the MP4/aug-cc-pVDZ level, β_μ(**7H**)<β_μ(**9H**) and the β_μ(**9H**)/β_μ(**7H**) ratio is ca. 5. Thus, based on the β_μ values, and anticipating future NLO studies, the low-energy keto tautomers of guanine could be identified through SHG measurements. On the other hand, when considering the intrinsic hyperpolarizabilities estimated via $\beta_{vec} = \sqrt{\beta_x^2 + \beta_y^2 + \beta_z^2}$, the values for the investigated tautomers are rather close to each other (within ca. 10 %). Upon analyzing the most important contributors to β_μ, it becomes clear that the difference between the **7H** and **9H** forms is mainly the magnitude and sign of the μ_y component: the MP4/aug-cc-pVDZ $\mu_y\beta_y/\mu$ values are calculated to be −50.6 and 54.5 a.u., respectively. Interestingly, the MP2/aug-cc-pVDZ β_μ values of both tautomers agree satisfactorily with the corresponding MP4/aug-cc-pVDZ data to within ca. 10 a.u. (Fig. 4), with the MP2/aug-cc-pVDZ β_μ(**9H**)/β_μ(**7H**) ratio being ca. 4. All of the DFT methods, especially the B3LYP/aug-cc-pVDZ level, reproduce the MP4/aug-cc-pVDZ β_μ(**7H**) datum reasonably well. By contrast, for the **9H** tautomer, the B3LYP, B97-1, and PBE1PBE functionals give small negative β_μ values, in disagreement with the results of the MP4 calculations (Fig. 4, Table 2). On the other hand, quite unlike the traditional functionals, the CAM-B3LYP level properly reproduces the sign of the β_μ(**7H**) value obtained by conventional ab initio methods, although β_μ(**7H**) is rather close to the value for the **9H** tautomer.

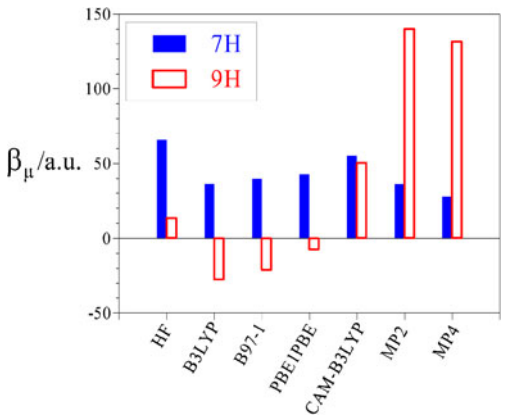

Fig. 4 Static electronic first-order hyperpolarizability of the guanine tautomers as a function of the level of calculation. Basis set: aug-cc-pVDZ

At the MP4/aug-cc-pVDZ level, the largest hyperpolarizability component for both isomers lies along the *x* axis. For the **7H** tautomer, the β_{xxx}, β_{yyy}, and β_{zzz} values are calculated to be 154.6, −20.0, and 0.5 a.u., respectively. The corresponding CAM-B3LYP/aug-cc-pVDZ data are 114.9, −55.2, and −0.5 a.u., respectively. The reason for these β_{iii} (i=x, y, z) was investigated by determining the spatial contributions of electrons to the hyperpolarizability components. We therefore performed a hyperpolarizability density analysis. Following the papers of Nakano and co-workers, the β density [$\rho^{(2)}(r)$] was defined as follows (r denotes the position vector) [92–94]:

$$\rho(r,F) = \rho^{(0)}(r) + \sum_j \rho_j^{(1)}(r)\,F_j + \frac{1}{2!}\sum_j \rho_{jk}^{(2)}(r)\,F_jF_k + \frac{1}{3!}\sum_j \rho_{jkl}^{(3)}(r)\,F_jF_kF_l + ... \quad (3)$$

$$\beta_{ijk} = -\frac{1}{2!}\int r\,\rho_{jk}^{(2)}(r)\,dr \quad (4)$$

$$\rho_{jk}^{(2)}(r) = \frac{\partial^2\rho(r,F)}{\partial F_j \partial F_k}\Big|_{F_j=0,F_k=0} \quad (5)$$

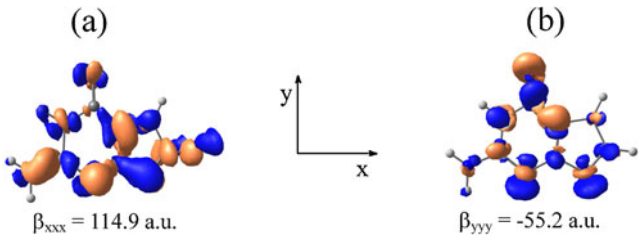

Fig. 5a–b Hyperpolarizability density distributions $\rho_{xx}^{(2)}(r)$ (**a**) and $\rho_{yy}^{(2)}(r)$ (**b**) of the **7H** tautomer of guanine. The *orange* and *blue* surfaces (see the color figure online) refer to positive and negative $\rho_{jj}^{(2)}(r)$ densities, respectively, computed at the isosurface of 10 a.u. CAM-B3LYP/aug-cc-pVDZ results are shown

When considering a pair of localized positive and negative $\rho_{jj}^{(2)}(r)$ densities, the magnitude of their contribution to β is proportional to the distance between them, while the sign is positive if the positive-to-negative $\rho_{jj}^{(2)}(r)$ direction coincides with the positive direction of the coordinate system. In the present work, the $\rho_{jj}^{(2)}(r)$ values were determined at the CAM-B3LYP/aug-cc-pVDZ level for the *xx* and *yy* components, adopting the numerical procedure described in [93]. Figure 5 shows the $\rho_{xx}^{(2)}(r)$ and $\rho_{yy}^{(2)}(r)$ distributions for the **7H** tautomer. The largest positive and negative $\rho_{xx}^{(2)}(r)$ contributions are mainly localized on the pyrimidine and imidazole rings, respectively, while the most significant $\rho_{yy}^{(2)}(r)$ amplitudes are localized on the pyrimidine moiety and near the nitrogen atom at position 9. As can be appreciated from the plots in Fig. 5, the positive and negative $\rho_{xx}^{(2)}(r)$ pairs are almost aligned along the positive *x* direction, in agreement with the sign of the β_{xxx} component (Table 1). On the other hand, the largest positive-to-negative $\rho_{yy}^{(2)}(r)$ amplitudes are oriented along the negative *y* direction, in line with the negative β_{yyy} value. In addition, both the $\rho_{xx}^{(2)}(r)$ amplitudes and the distance between the positive and negative *xx* densities are greater than those for the $\rho_{yy}^{(2)}(r)$ pairs, consistent with $|\beta_{xxx}|>|\beta_{yyy}|$.

Conclusions

In this work, dipole moments, charge distributions, and electronic hyperpolarizabilities of the neutral lowest-energy keto **7H** and **9H** tautomers of guanine in the gas phase were calculated using HF, MP*n* (n=2 and 4), and a variety of DFT methods. The effects of augmenting the basis set (aug-cc-pVDZ→ *d*-aug-cc-pVDZ) on the calculated properties were found to be rather modest. The dipole moments were barely dependent on the computational level applied, whereas the magnitude and sign of the first-order hyperpolarizability were rather sensitive to the theoretical method employed. The results show that the magnitude and direction of the dipole moment and the first-order hyperpolarizability change noticeably between the **7H** and **9H** isomers. Specifically, at the highest correlated MP4/aug-cc-pVDZ level, the μ(**9H**)/μ(**7H**) and β_μ(**9H**)/β_μ(**7H**) ratios were predicted to be ca. 3.5 and 5, respectively. Therefore, μ and β_μ could potentially be helpful when attempting to discriminate between the most stable keto tautomers of guanine, unlike the electronic polarizabilities and second-order hyperpolarizabilities, which are barely influenced by the **7H**/**9H** tautomerization [47]. Among the DFT functionals tested, the CAM-B3LYP method provides the best agreement with the MP4 level. The sign and magnitude of the largest diagonal β_{iii} components of the **7H** tautomer were confirmed by performing hyperpolarizability density analyses.

References

1. Lin J, Miller J, Miller E (1977) 2,3-Dihydro-2-(guan-7-yl)-3-hydroxy-aflatoxin B1, a major acid hydrolysis product of aflatoxin B1-DNA or -ribosomal RNA adducts formed in hepatic microsome-mediated reactions and in rat liver in vivo. Cancer Res 37:4430–4438
2. Bailey EA, Iyer RS, Harris TM, Essigmann JM (1996) A viral genome containing an unstable aflatoxin B1-N7-guanine DNA adduct situated at a unique site. Nucl Acids Res 24:2821–2828
3. Watson JD, Crick FH (1953) Molecular structure of nucleic acids: a structure for deoxyribose nucleic acid. Nature 171:737–738
4. Topal MD, Fresco JR (1976) Complementary base pairing and the origin of substitution mutations. Nature 263:285–289
5. Harris VH, Smith CL, Cummins WJ, Hamilton AL, Adams H, Dickman M, Hornby DP, Williams DM (2003) The effect of tautomeric constant on the specificity of nucleotide incorporation during DNA replication: support for the rare tautomer hypothesis of substitution. J Mol Biol 326:1389–1401
6. Hanus M, Ryjacek F, Kabelac M, Kubar T, Bogdan TV, Trygubenko SA, Hobza P (2003) Correlated ab initio study of nucleic acid bases and their tautomers in the gas phase, in a microhydrated environment and in aqueous solution. Guanine: surprising stabilization of rare tautomers in aqueous solution. J Am Chem Soc 125:7678–7688
7. Nir E, Janzen C, Imhof P, Kleinermanns K, de Vries MS (2001) Guanine tautomerism revealed by UV–UV and IR–UV hole burning spectroscopy. J Chem Phys 115:4604–4611
8. Shukla MK, Leszczynski J (2006) Spectral origins and ionization potentials of guanine tautomers: theoretical elucidation of experimental findings. Chem Phys Lett 429:261–265
9. Seefeld K, Brause R, Häber T, Kleinermanns K (2007) Imino tautomers of gas-phase guanine from mid-infrared laser spectroscopy. J Phys Chem A 111:6217–6221
10. Kushwaha PS, Kumar A, Mishra PC (2004) Electronic transitions of guanine tautomers, their stacked dimers, trimers and sodium complexes. Spectrochim Acta A 60:719–728
11. Piacenza M, Grimme S (2004) Systematic quantum chemical study of DNA-base tautomers. J Comput Chem 25:83–99
12. Haranczyk M, Gutowski M (2005) Valence and dipole-bound anions of the most stable tautomers of guanine. J Am Chem Soc 127:699–706
13. Jang YH, Goddard WA III, Noyes KT, Sowers LC, Hwang S, Chung DS (2003) pK_a values of guanine in water: density functional theory calculations combined with Poisson–Boltzmann continuum–solvation model. J Phys Chem B 107:344–357
14. Shukla MK, Leszczynski J (2005) Excited state proton transfer in guanine in the gas phase and in water solution: a theoretical study. J Phys Chem A 109:7775–7780
15. Bravaya KB, Kostko O, Dolgikh S, Landau A, Ahmed M, Krylov AI (2010) Electronic structure and spectroscopy of nucleic acid bases: ionization energies, ionization-induced structural changes, and photoelectron spectra. J Phys Chem A 114:12305–12317
16. Mennucci B, Toniolo A, Tomasi J (2001) Theoretical study of guanine from gas phase to aqueous solution: role of tautomerism and its implications in absorption and emission spectra. J Phys Chem A 105:7126–7134
17. Jones DB, Wang F, Winkler DA, Brunger MJ (2006) Orbital based electronic structural signatures of the guanine keto G-7H/G-9H tautomer pair as studied using dual space analysis. Biophys Chem 121:105–120
18. Gorb L, Kaczmarek A, Gorb A, Sadlej AJ, Leszczynski J (2005) Thermodynamics and kinetics of intramolecular proton transfer in guanine. Post Hartree–Fock study. J Phys Chem B 109:13770–13776

19. Liang W, Li H, Hu X, Han S (2006) Systematic theoretical investigations on all of the tautomers of guanine: from both dynamics and thermodynamics viewpoint. Chem Phys 328:93–102
20. Mons M, Dimicoli I, Piuzzi F, Tardivel B, Elhanine M (2002) Tautomerism of the DNA base guanine and its methylated derivatives as studied by gas-phase infrared and ultraviolet spectroscopy. J Phys Chem A 106:5088–5094
21. Chin W, Mons M, Dimicoli I, Piuzzi F, Tardivel B, Elhanine M (2002) Tautomer contributions to the near UV spectrum of guanine: towards a refined picture for the spectroscopy of purine molecules. Eur Phys J D 20:347–355
22. Sheina GG, Stepanian SG, Radchenko ED, Blagoi YP (1987) IR spectra of guanine and hypoxanthine isolated molecules. J Mol Struct 158:275–292
23. Choi MY, Miller RE (2006) Four tautomers of isolated guanine from infrared laser spectroscopy in helium nanodroplets. J Am Chem Soc 128:7320–7328
24. Nir E, Plutzer C, Kleinermanns K, de Vries M (2002) Properties of isolated DNA bases, base pairs and nucleosides examined by laser spectroscopy. Eur Phys J D 20:317–329
25. Nir E, Grace L, Brauer B, de Vries MS (1999) REMPI spectroscopy of jet-cooled guanine. J Am Chem Soc 121:4896–4897
26. Nir E, Kleinermanns K, Grace L, de Vries MS (2001) On the photochemistry of purine nucleobases. J Phys Chem A 105:5106–5110
27. Piuzzi F, Mons M, Dimicoli I, Tardivel B, Zhao Q (2001) Ultraviolet spectroscopy and tautomerism of the DNA base guanine and its hydrate formed in a supersonic jet. Chem Phys 270:205–214
28. Chin W, Mons M, Piuzzi F, Tardivel B, Dimicoli I, Gorb L, Leszczynski J (2004) Gas phase rotamers of the nucleobase 9-methylguanine enol and its monohydrate: optical spectroscopy and quantum mechanical calculations. J Phys Chem A 108:8237–8243
29. Mons M, Piuzzi F, Dimicoli I, Gorb L, Leszczynski J (2006) Near-UV resonant two-photon ionization spectroscopy of gas phase guanine: evidence for the observation of three rare tautomers. J Phys Chem A 110:10921–10924
30. Steckl AJ (2007) DNA—a new material for photonics? Nature Photon 1:3–5
31. Guerra CF, van der Wijst T, Bickelhaupt FM (2006) Nanoswitches based on DNA base pairs: why adenine–thymine is less suitable than guanine–cytosine. Chem Phys Chem 7:1971–1979
32. Endres RG, Cox DL, Singh RRP (2004) The quest for high-conductance DNA. Rev Mod Phys 76:195–214
33. Yan H, Zhang X, Shen Z, Seeman NE (2002) A robust DNA mechanical device controlled by hybridization topology. Nature 415:62–65
34. Porath D, Cuniberti G, Felice RD (2004) Charge transport in DNA based devices. In: Schuster G (ed) Long range charge transfer in DNA. Topics in current chemistry, vol 237. Springer, Heidelberg, pp 183–227
35. Coehn H, Nogues C, Naaman R, Porath D (2005) Direct measurement of electrical transport through single DNA molecules of complex sequence. Proc Natl Acad Sci USA 102:11589–11593
36. Di Felice R, Calzolari A, Molinari E, Garbesi A (2002) Ab initio study of model guanine assemblies: the role of π–π coupling and band transport. Phys Rev B 65:045104–045113
37. Cohen H, Sapir T, Borovok N, Molotsky T, Di Felice R, Kotlyar AB, Porath D (2007) Polarizability of G4-DNA observed by electrostatic force microscopy measurements. Nano Lett 7:981–986
38. Wang L, Yoshida J, Ogata N (2001) Self-assembled supramolecular films derived from marine deoxyribonucleic acid (DNA)-cationic surfactant complexes: large-scale preparation and optical and thermal properties. Chem Mater 13:1273–1281
39. Grote JG, Hagen JA, Zetts JS, Nelson RL, Diggs DE, Stone MO, Yaney PP, Heckman E, Zhang C, Steier WH, Jen AK-Y, Dalton LR, Ogata N, Curley MJ, Clarson SJ, Hopkins FK (2004) Investigation of polymers and marine-derived DNA in optoelectronics. J Phys Chem B 108:8584–8591
40. Bottcher CFJ (1952) Theory of electric polarization. Elsevier, Amsterdam
41. Haley TP, Graybill ER, Cybulski SM (2006) Ab initio calculations of dispersion coefficients for nucleic acid base pairs. J Chem Phys 124:204301, 1–7
42. Campos CT, Jorge FE (2009) Basis set convergence of electric properties in HF and DFT calculations of nucleic acid bases. Int J Quantum Chem 109:285–293
43. Labello NP, Ferreira AM, Kurtz HA (2005) An augmented effective core potential basis set for the calculation of molecular polarizabilities. J Comput Chem 26:1464–1471
44. Jasien PG, Fitzgerald G (1990) Molecular dipole moments and polarizabilities from local density functional calculations: application to DNA base pairs. J Chem Phys 93:2554–2560
45. Johnson RC, Power TD, Holt JS, Immaraporn B, Monat JE, Sissoko AA, Yanik MM, Zagorodny AV, Cybulski SM (1996) Electron-correlated calculations of electric properties of nucleic acid bases. J Phys Chem 100:18875–18881
46. Basch H, Garmer DR, Jasien PG, Krauss M, Stevens WJ (1989) Electrical properties of nucleic acid bases. Chem Phys Lett 163:514–522
47. Alparone (2013) Linear and nonlinear optical properties of nucleic acid bases. Chem Phys 410:90–98
48. Salafsky JS (2003) Second-harmonic generation as a probe of conformational change in molecules. Chem Phys Lett 381:705–709
49. Sliwa M, Nakatani K, Asahi T, Lacroix PG, Pansu RB, Masuhara H (2007) Polarization and wavelength dependent nonlinear optical properties of a photo-switchable organic crystal. Chem Phys Lett 437:212–217
50. Sliwa M, Létard S, Malfant I, Nierlich M, Lacroix PG, Asahi T, Masuhara H, Yu P, Nakatani K (2005) Design, synthesis, structural and nonlinear optical properties of photochromic crystals: toward reversible molecular switches. Chem Mater 17:4727–4735
51. Alparone A (2012) Dipole (hyper)polarizabilities of fluorinated benzenes: an ab initio investigation. J Fluorine Chem 144:94–101
52. Velders GJM, Gillet JM, Becker PJ, Feil D (1991) Electron density analysis of nonlinear optical materials: an ab initio study of different conformations of benzene derivatives. J Phys Chem 95:8601–8608
53. Hendrickx E, Clays K, Persoons A, Dehu C, Bredas JL (1995) The bacteriorhodopsin chromophore retinal and derivatives: an experimental and theoretical investigation of the second-order optical properties. J Am Chem Soc 117:3547–3555
54. Alparone A, Millefiori A, Millefiori S (2005) Electronic dipole polarizability and hyperpolarizability of formic acid. Chem Phys Lett 409:288–294
55. Niewodniczański W, Bartkowiak W (2007) Theoretical study of geometrical and nonlinear optical properties of pyridinum N-phenolate betaine dyes. J Mol Model 13:793–800
56. Xu H-L, Li Z-R, Su Z-M, Muhammad S, Gu FL, Harigaya K (2009) Knot-isomers of Mobius cyclacene: how does the number of knots influence the structure and first hyperpolarizability? J Phys Chem C 113:15380–15383
57. Plaquet A, Champagne B, Castet F, Ducasse L, Bogdan E, Rodriguez V, Pozzo J-L (2009) Theoretical investigation of the dynamic first hyperpolarizability of DHA-VHF molecular switches. New J Chem 33:1349–1356
58. Lipiński J, Bartkowiak W (1999) Conformation and solvent dependence of the first and second molecular hyperpolarizabilities of charge-transfer chromophores. Quantum-chemical calculations. Chem Phys 245:263–276
59. Seal P, Jha PC, Chakrabarti S (2008) Static first order hyperpolarizabilities of DNA base pairs: a configuration interaction study. J Mol Struct (THEOCHEM) 855:64–68

60. Champagne B, Perpete EA, van Gisbergen SJA, Baerends E-J, Snijders JG, Soubra-Ghaoui C, Robins KA, Kirtman B (1998) Assessment of conventional density functional schemes for computing the polarizabilities and hyperpolarizabilities of conjugated oligomers: an ab initio investigation of polyacetylene chains. J Chem Phys 109:10489–10498
61. Kamiya M, Sekino H, Tsuneda T, Hirao K (2005) Nonlinear optical property calculations by the long-range-corrected coupled-perturbed Kohn–Sham method. J Chem Phys 122:234111, 1–10, and references therein
62. Lee C, Yang W, Parr RG (1988) Development of the Colle–Salvetti correlation energy formula into a functional of the electron density. Phys Rev B 37:785–789
63. Becke AD (1993) A new mixing of Hartree–Fock and local density-functional theories. J Chem Phys 98:1372–1377
64. Perdew JP (1997) Burke K, Ernzerhof M (1997) Generalized gradient approximation made simple. Phys Rev Lett 78:1396–1396
65. Hamprecht FA, Cohen AJ, Tozer DJ, Handy NC (1998) Development and assessment of new exchange-correlation functional. J Chem Phys 109:6264–6271
66. Yanai T, Tew D, Handy NC (2004) A new hybrid exchange–correlation functional using the Coulomb-attenuating method (CAM-B3LYP). Chem Phys Lett 393:51–57
67. Jacquemin D, Perpète EA, Scalmani G, Frisch MJ, Kobayashi R, Adamo C (2007) Assessment of the efficiency of long-range corrected functionals for some properties of large compounds. J Chem Phys 126:144105, 1-12
68. Limacher PA, Mikkelsen KV, Lüthi HP (2009) On the accurate calculation of polarizabilities and second hyperpolarizabilities of polyacetylene oligomer chains using the CAM-B3LYP density functional. J Chem Phys 130:194114, 1-7
69. Nakano M, Minami T, Fukui H, Yoneda K, Shigeta Y, Kishi R, Champagne B, Botek E (2010) Approximate spin-projected spin-unrestricted density functional theory method: application to the diradical character dependences of the (hyper)polarizabilities in *p*-quinodimethane models. Chem Phys Lett 501:140–145
70. Alparone A (2011) Comparative study of CCSD(T) and DFT methods: electronic (hyper)polarizabilities of glycine. Chem Phys Lett 514:21–25
71. Zhang C-C, Xu H-L, Hu Y-Y, Sun S-L, Su Z-M (2011) Quantum chemical research on structures, linear and nonlinear optical properties of the Li@*n*-acenes salt (*n*=1, 2, 3, and 4). J Phys Chem A 115:2035–2040
72. Alparone A (2012) Structural, energetic and response electric properties of cyclic selenium clusters: an ab initio and density functional theory study. Theor Chem Acc 131:1239, 1–14
73. Alparone A, Librando V (2012) Physicochemical characterization of environmental mutagens: 3-nitro-6-azabenzo[a]pyrene and its N-oxide derivative. Monatsh Chem 143:1123–1132
74. Krawczyk P (2010) DFT study of linear and nonlinear optical properties of donor–acceptor substituted stilbenes, azobenzenes and benzilideneanilines. J Mol Model 16:659–668
75. Frisch MJ, Trucks GW, Schlegel HB, Scuseria GE, Robb MA, Cheeseman JR, Scalmani G, Barone V, Mennucci B, Petersson GA, Nakatsuji H, Caricato M, Li X, Hratchian HP, Izmaylov AF, Bloino J, Zheng G, Sonnenberg JL, Hada M, Ehara M, Toyota K, Fukuda R, Hasegawa J, Ishida M, Nakajima T, Honda Y, Kitao O, Nakai H, Vreven T, Montgomery JA Jr, Peralta JE, Ogliaro F, Bearpark M, Heyd JJ, Brothers E, Kudin KN, Staroverov VN, Kobayashi R, Normand J, Raghavachari K, Rendell A, Burant JC, Iyengar SS, Tomasi J, Cossi M, Rega N, Millam JM, Klene M, Knox JE, Cross JB, Bakken V, Adamo C, Jaramillo J, Gomperts R, Stratmann RE, Yazyev O, Austin AJ, Cammi R, Pomelli C, Ochterski JW, Martin RL, Morokuma K, Zakrzewski VG, Voth GA, Salvador P, Dannenberg JJ, Dapprich S, Daniels AD, Farkas, Foresman JB, Ortiz JV, Cioslowski J, Fox DJ (2009) Gaussian 09, revision A.02. Gaussian Inc., Wallingford
76. Schmidt MW, Baldridge KK, Boatz JA, Elbert ST, Gordon MS, Jensen JH, Koseki S, Matsunaga N, Nguyen KA, Su SJ, Windus TL, Dupuis M, Montgomery JA (1993) General atomic and molecular electronic structure system. J Comput Chem 14:1347–1363
77. Dunning TH (1989) Gaussian basis sets for use in correlated molecular calculations. I. The atoms boron through neon and hydrogen. J Chem Phys 90:1007–1023
78. Burcl R, Handy NC, Carter S (2003) Vibrational spectra of furan, pyrrole, and thiophene from a density functional theory anharmonic force field. Spectrochim Acta A 59:1881–1893
79. Millefiori S, Alparone A (2004) Tautomerism and polarizability in uracil: coupled cluster and density-functional theory study. Chem Phys 303:27–36
80. Alparone A, Millefiori A, Millefiori S (2005) Non-planarity and solvent effects on structural and polarizability properties of cytosine tautomers. Chem Phys 312:261–274
81. Clowney L, Jain SC, Srinivasan AR, Westbrook J, Olson WK, Berman HM (1996) Geometric parameters in nucleic acids: nitrogenous bases. J Am Chem Soc 118:509–518
82. Karna SP, Dupuis M (1991) Frequency dependent nonlinear optical properties of molecules: formulation and implementation in the HONDO program. J Comput Chem 12:487–504
83. Kurtz HA, Stewart JJP, Dieter KM (1990) Calculation of the nonlinear optical properties of molecules. J Comput Chem 11:82–87
84. Woon DE, Dunning TH (1994) Gaussian basis sets for use in correlated molecular calculations. IV. Calculation of static electrical response properties. J Chem Phys 100:2975–2988
85. Alparone A (2011) Theoretical study of the electronic (hyper)polarizabilities of amino acids in gaseous and aqueous phases. Comput Theor Chem 976:188–190
86. Alparone A (2012) Corrigendum to "Theoretical study of the electronic (hyper)polarizabilities of amino acids in gaseous and aqueous phases" [Comput. Theor. Chem. 976 (2011) 188–190]. Comput Theor Chem 980:144–144
87. Millefiori S, Alparone A (1998) Ab initio and density functional theory calculations of the dipole polarizabilities of ethene, benzene and naphthalene. J Mol Struct (THEOCHEM) 422:179–190
88. Librando V, Alparone A, Minniti Z (2008) Computational study on dipole moment, polarizability and second hyperpolarizability of nitronaphthalenes. J Mol Struct (THEOCHEM) 856:105–111
89. Millefiori S, Alparone A, Millefiori A, Vanella A (2008) Electronic and vibrational polarizabilities of the twenty naturally occurring amino acids. Biophys Chem 132:139–147
90. Párkányi C, Boniface C, Aaron J-J, Bulaceanu-MacNairb M, Dakkouri M (2002) Theoretical and experimental dipole moments of purines. Collect Czech Chem Commun 67:1109–1124
91. Reed AE, Weinstock RB, Weinhold F (1985) Natural population analysis. J Chem Phys 83:735–746
92. Nakano M, Shigemoto I, Yamada S, Yamaguchi K (1995) Size–consistent approach and density analysis of hyperpolarizability: second hyperpolarizabilities of polymeric systems with and without defects. J Chem Phys 103:4175–4191
93. Yamada S, Nakano M, Shigemoto I, Kiribayashi S, Yamaguchi K (1997) Intense electron correlation dependence of the first hyperpolarizabilities β of a nitroxide radical and formaldehyde. Chem Phys Lett 267:445–451
94. Nakano M, Ohta S, Tokushima K, Kishi R, Kubo T, Kamada K, Ohta K, Champagne B, Botek E, Takahashi H (2007) First and second hyperpolarizabilities of donor–acceptor disubstituted diphenalenyl radical systems. Chem Phys Lett 443:95–101